JOURNAL OF SPACECRAFT AND ROCKETS
Vol. 30, No. 1, January-February 1993

Parametric Analysis of Radiative Structure in Aerobrake Shock Layers

Robert B. Greendyke*
ViGYAN, Inc., Hampton, Virginia 23666

A broad-spectrum version of the NEQAIR code was adapted for use in the radiative transfer equation by utilizing internally calculated absorption and emission coefficients and applied to aerobrake flowfields calculated by the LAURA code with a variety of kinetic models. The resulting radiative fluxes were obtained in a decoupled fashion from the flowfield solver along the vehicle's stagnation streamline. The radiative flux obtained was broken down by causative process to study the radiative structure for the various kinetic models. In addition, the radiative fluxes for several points on a typical aeroassist trajectory were analyzed to examine how the radiative structure changes as the vehicle completes its aeropass. Atomic nitrogen and N_2^+ first negative radiative processes dominated the stagnation radiative flux, and the flowfield conditions near the wall were found to exert considerable influence over the radiative flux to the wall.

Nomenclature

a = thermal exponent used in Eq. (4), usually equal to 0.3, but redefined by Eq. (5)
b = thermal exponent used in Eq. (4), usually equal to 0.7, but redefined by Eq. (6)
e_λ = radiative emission coefficient, W/cm^3-μ-sr
$\hat{I}$ = ionization potential energy, eV
I_λ = specific radiative intensity, W/cm^3-μ-sr
$I_{\lambda 0}$ = specific radiative intensity from adjacent gas layer, W/cm^3-μ-sr
I' = incident radiative flux as defined in Eq. (8)
T_{ave} = average temperature as defined by Eq. (4), K
T_e = electron temperature, K
T_H = heavy particle translational temperature, K
T_V = heavy particle vibrational temperature, K
z = gas layer thickness in direction normal to body surface, cm
α'_λ = radiative absorption coefficient corrected for stimulated emission, cm^{-1}
λ = wavelength, Å
σ_V = limiting vibrational excitation cross section, m^2

Introduction

IN the near future, aerobraking will be employed on a variety of vehicles to allow them to enter or make a transition within Earth orbit in an economical fashion. Nonequilibrium radiative heating will be an important contribution to the overall heat transfer these vehicles will experience. Unfortunately, radiative heat transfer is not fully understood as a phenomena. Several computer codes exist[1-3] that calculate nonequilibrium radiative heat transfer with varying degrees of computational complexity. The most detailed method is the NEQAIR[1] code of Park. The NEQAIR code has been used in the past primarily with the thin-gas assumption that self-absorption above 2000 Å is negligible and all flux below this point would be absorbed in the shock layer. In the present study, the emission and absorption coefficients in the NEQAIR code will be utilized in the radiative transfer equation to obtain a broad-spectrum version of the NEQAIR code that includes self-absorption.

All radiative heat transfer models are affected by the local thermodynamic conditions in the flowfield, and it is important to understand how the various differences in flowfield assumptions can affect the calculation of radiative heat transfer. In this paper a sensitivity study will be conducted in which the influence of ionization potential, chemical rate models, and the limiting value of vibrational excitation cross sections on the calculation of noncoupled, absorbing, broad-spectrum radiative transfer and structure will be examined. In addition, an analysis of how the radiative structure changes with altitude and velocity variations will be conducted. It is well known that the radiative flux will vary in magnitude through a trajectory, but it has not been established how the individual radiative processes are influenced by freestream variations.

Method

The Langley Aerothermodynamic Upwind Relaxation Algorithm (LAURA) code[5,6] was used throughout this study for the simulation of an aerobrake in an axisymmetric fashion. These same flowfields had been utilized in a previous study of electron number density profiles for an aerobrake vehicle,[7] and the present paper is a continuation of that work. The LAURA code is a point-implicit relaxation algorithm for obtaining the numerical solution to the governing equations for viscous hypersonic flows in chemical and thermal nonequilibrium. The algorithm is derived using a finite volume formulation in which the inviscid components of the flux across cell walls are described with Roe's averaging[8] and Harten's entropy fix[9] with second-order corrections based on Yee's symmetrical total variation diminishing scheme.[10,11] The code includes 11 species continuity equations, 3 momentum equations, and 1 energy equation each for both the vibrational-electronic and total energies. The vibrational and electronic energies of all species are assumed to be in equilibrium at a temperature T_V and the translational and rotational energies in equilibrium at temperature T_H. Stewart's finite rate catalytic wall boundary condition[12] was incorporated into the solution routine for all cases.

In the first section of this paper we will consider the variation of three main kinetic model parameters and their influence on the radiative structure and flux along the stagnation streamline. The first, identified by I, is the reference value of the ionization potential $\hat{I}$. The number following I in the case identifier denotes which set of reference values were used. The primary ($I = 1$) set of ionization potentials represents the en-

Received May 7, 1992; presented as Paper 92-2970 at the AIAA 23rd Plasmadynamics and Lasers Conference, Nashville, TN, July 6-8, 1992; revision received Aug. 17, 1992; accepted for publication Aug. 19, 1992.

*Research Engineer. Member AIAA.

ergy required to ionize an atom from an already excited state, whereas the secondary ($I=2$) set of potentials are the ionization potentials measured from the ground state of the given species. Thus, $\hat{I}(\mathrm{N})=4.196$ eV and $\hat{I}(\mathrm{O})=4.453$ eV for $I=1$, and $\hat{I}(\mathrm{N})=14.53$ eV and $\hat{I}(\mathrm{O})=13.614$ eV for $I=2$. The second parameter varied is the choice of chemical rates and is identified by K. The choices, in numerical order from $K=1$ to 3, are 1) the rates of Kang and Dunn,[13] 2) the rates used by Park (1987)[14] with recent updates, and 3) Park's (1990) rates.[15] There is considerable difference between the three models not only in the reaction rates but also in the reactions considered. The final parameter, identified by S, is the value of the limiting cross section for vibrational excitation or σ_V. The first option ($S=1$) is the curve fit value of Park,[14] where

$$\sigma_V = 1\times 10^{-17}\left(\frac{50{,}000}{T_H}\right)^2 \tag{1}$$

The second option ($S=2$) is the constant value of the limiting cross section chosen for this parametric study where

$$\sigma_V = 1\times 10^{-16} \tag{2}$$

The third option ($S=3$) is another constant value of the limiting cross section

$$\sigma_V = 1\times 10^{-17} \tag{3}$$

The $S=2$ and 3 options roughly bound the expression given in Eq. (1). Every variation of the kinetic model can then be denoted by a six-digit identifier where I1K2S1 denotes the baseline condition of ionization from the excited state, Park's (1987) chemical rates,[14] and Park's curve fit for the limiting cross section for vibrational excitation.

Throughout this study, the LAURA code was used to solve for the flowfields around an equivalent sphere with a nose radius of 2.16 m. The computational grid utilized for all solutions in the first section had 64 cells in the direction normal to the body and 32 cells along the surface of the body. The flowfields obtained for the study of kinetic model parameter variations were solved at the freestream conditions listed as point 1 in Table 1. The wall temperature for all cases was set by user input to 1750 K, the temperature at which reactive cured glass (RCG) tile coatings begin to soften.

In the second portion of this study, a parametric examination was made of the radiative structure of the shock layer as altitude was varied (points 2–5 of Table 1). It is a well-established fact that the total radiative flux to a vehicle will vary as a function of the vehicle's altitude and velocity, but it is not well known how the qualitative radiative structure will change. The aim of this portion of the study was to determine how the radiative structure would vary through the trajectory.

Utilizing the same flowfields calculated for an earlier study of electron number densities,[7] the baseline kinetic model was improved following the suggestions of Hansen[16] wherein the exponents of Park's rate controlling temperature[14]

$$T_{\mathrm{ave}} = T_V^a \times T_H^b \tag{4}$$

where a and b that had been $a=0.3$ and $b=0.7$ were replaced[7] by

$$a = \left[0.1+0.4\times\left(\frac{T_V}{T_H}\right)\right] \tag{5}$$

and

$$b = 1-a \tag{6}$$

Although these updates to the LAURA code made quantitative changes in the flowfield,[7] their effect on the radiative flux and structure was found to be negligible. The total number density was utilized in place of the species number density in Eq. (56) of Ref. 5 to reflect true collisional probabilities. The various flowfield parameters examined in the first section were held constant at their baseline (I1K2S1) values whereas the altitude was varied. The computational grid for trajectory variation had 128 cells in the direction normal to the body and 30 cells circumferentially.

Table 1 Trajectory points

Point	Time, s	Altitude, km	Velocity, km/s	Density kg/m^3	Temperature K
1	——	78.46	9.688	2.484×10^{-5}	197.3
2	70	82.96	9.848	1.160×10^{-5}	193.9
3	110	76.47	9.418	3.412×10^{-5}	198.5
4	150	75.03	8.744	4.323×10^{-5}	199.5
5	190	76.15	8.145	3.595×10^{-5}	198.7

The NEQAIR code calculates the population distribution of atoms and molecules among their states by use of a quasi-steady-state assumption.[14] The assumption assumes that the rate at which an electronic state is populated or depopulated greatly exceeds the difference between the two rates and therefore the difference can be ignored. With known population rates, the number densities of the electronic states can then be calculated by matrix inversion given the known thermodynamic conditions at the local point in the flowfield. The NEQAIR code then calculates the radiative emission and absorption coefficients on a line-by-line basis over the spectral region specified.

For this investigation, the spectral region considered was between 800 and 15,000 Å. The absorbing radiative flux was calculated by assuming that each grid point constituted a thermodynamically homogeneous layer. The radiative intensity, as a function of wavelength at each point, is then[17]

$$I_\lambda = \left(\frac{e_\lambda}{\alpha'_\lambda}\right)\times(1-e^{-\alpha'_\lambda z})+I_{\lambda 0}e^{-\alpha'_\lambda z} \tag{7}$$

The radiative flux throughout the flowfield can then be integrated over a 2π sr solid angle and the wavelength interval of the spectral segment under consideration to obtain the incident radiative flux,

$$I' = \int_0^{2\pi}\int_{\lambda\min}^{\lambda\max} I_\lambda \, d\lambda \, d\theta \tag{8}$$

in a marching fashion from the shock to the wall.

The contributions of individual radiative processes to the overall radiative transfer were obtained by first solving for the incident radiative flux with all radiative processes intact at each spacial grid location. This information was retained at each grid location as a control and is displayed as the "Total" value in all figures presented. The calculation was then repeated with the contribution of individual processes to the overall emission coefficient, but not the absorption coefficient, deleted in the NEQAIR code and the resulting incident flux retained at each grid point. The difference was then taken between these incident radiative fluxes and the control for each case to determine the contribution of individual radiative processes.

In the NEQAIR code several radiative process are accounted for. Atomic radiative processes include bound-bound, bound-free, and free-free transitions for both nitrogen and oxygen. Molecular band systems included are the N_2^+ first negative, N_2 first positive, second positive, and Lyman-Birge-Hopfield bands, NO β, NO γ, and O_2 Schumann-Runge. All atomic processes were combined to reflect the contribution of individual species. At the onset of this project it was found that bound-bound processes dominated the incident radiative flux resulting from atoms for the current calculations. It was felt that little would be gained by separation of the three

modes of atomic radiation and doing so would incur considerable computational effort. A spectral array size of 20,000 points was used for this study. The assumption was made in both the LAURA and NEQAIR codes that vibrational-electronic temperature and temperature of free electrons are closely coupled, and therefore the assumption that $T_e = T_V$ was made throughout this study. In addition to radiative properties, a simple modification of the NEQAIR code yielded population densities for the electronic states under consideration to provide a better understanding of the radiative phenomena.

Two factors that were not considered in this study need to be mentioned. The first is wall catalysis. No variation of the wall catalysis model was felt to be necessary for this study. Although catalysis might have an influence on the magnitude of the radiative flux reaching the wall, this influence would only be observed in the cells closest to the wall. The patterns observed in this study, with the exception of inner thermal layer transparency, started far enough into the shock layer that it can be assumed that they were not affected by wall catalysis. In addition, most of the radiative flux reaching the wall in this study was above 2000 Å in wavelength. Regardless of the wall catalysis model used, the flowfields would be virtually transparent to radiation in this spectral region and it is felt that catalysis would have had little influence on the observed results. The second factor not considered in this study is the effect of coupling the radiative heating to the energy equation. It was simply beyond the scope of this project to do so. It is felt that this would also be an unnecessary step in the study of similar flowfields due to the low magnitude of radiative flux relative to the total enthalpy in the flowfield itself.

Results

Some general comments about the results need to be made before they are examined on a case-by-case basis. The NEQAIR code is a very detailed approach to the problem of solving radiative heat transfer in hypersonic nonequilibrium flows. Unfortunately, it is computationally intensive and costly. The solution of a single stagnation streamline with 64 points between wall and freestream required approximately 20 min of Cray YMP CPU time with all radiative processes intact. It was noted in the course of this study that the code is also very sensitive to machine accuracy. The 64-bit accuracy of both the Cray 2 and Cray YMP was necessary to obtain solutions through the boundary-layer region. All other machines failed to successfully invert the matrix when solving for the state populations in this flow region according to the quasi-steady-state (QSS) assumption.

As we examine the results shown in Figs. 1–7, it is important to note two things about the figures. First, although the data were obtained or calculated for a large number of points along the stagnation streamline, for the sake of graphic clarity not all of those points are displayed in the figures. In all cases, except where trajectory was varied, every second point was plotted. Every third point was plotted in Fig. 7 due to the large (128) number of points normal to the surface. Second, the incident radiative flux I' is the radiative flux from one gas layer to the next and, as such, can be thought of as a "running total." In other words, as the magnitude of the flux increases, emission is greater than absorption; as the magnitude decreases, absorption dominates the radiative structure.

Finally, as shall soon be shown, atomic oxygen radiative processes contributed little to the overall radiative flux seen in all of the following cases. At the onset of this study it was found that, although atomic oxygen was not a dominant radiator, it functioned in the flowfield as a net radiative absorber. In other words, if both the emission and absorption coefficients for atomic oxygen were deleted from the total flux calculation, the total flux to the wall would increase. This point needs to be made when the influence of individual radiative processes is considered.

Kinetic Model Variations

Inspection of Figs. 1a–1f indicates that few of the band systems calculated by the NEQAIR code contribute significantly to the overall radiative flux at the freestream conditions given at point 1 of Table 1 or at any other conditions. The diatomic oxygen, NO bands, and the N_2 first positive and Lyman-Birge-Hopfield bands yielded only trace incident radiative fluxes. The N_2 second positive band yielded significant radiative flux in only one case, the I1K3S1 or Park's (1990) chemical rate case.[15] The primary reason for the lack of significant radiative flux from diatomic oxygen and nitric oxide is their low species number densities in the present flowfields. N_2^+ similarly appears in the flowfields in small quantities, but as can be seen in Figs. 1a–1f, the N_2^+ first negative band resulting from $B^2\Sigma \rightarrow$ ground state transitions is a strong radiator.

In all cases studied, the radiation resulting from atomic nitrogen processes dominated the radiative structure of the shock layers studied. Onset of atomic radiation was rapid, yet typically it peaked only halfway through the shock layer and was followed by rapid absorption as the boundary layer was reached at approximately 3 cm from the wall. Although atomic nitrogen radiation was strongly absorbed, it is interesting to note that at 0.5 cm from the wall all flowfields became transparent to atomic nitrogen processes. The only two things common to all flowfields that could account for this phenomenon are the wall temperature boundary condition inherent in the LAURA code and the use of Stewart's finite rate catalytic wall boundary condition.[12] The LAURA code assumes at the wall that the $T_H = T_V = T_{\text{wall}}$, where T_{wall} is set by the user in the LAURA input file. As stated, this value was set at 1750 K for all of the cases presented in this study.

Additionally, all of the cases utilizing either of Park's chemical rates and Park's curve fit for the limiting cross section for vibrational excitation produced a rapid peak in the atomic nitrogen flux in the immediate postshock region of the flowfield followed by rapid reabsorption. A second peak would then form of greater magnitude yielding a dual-peak profile. It is felt that the rapid initial ionization produced by both the Kang and Dunn chemical rates and the S2 limiting vibrational cross section (refer to Ref. 7, Figs. 4b and 4c) in this part of the flowfield consumes much of the energy that would have otherwise excited the nonionic atomic nitrogen and have been released by bound-bound transitions.

Virtually all of the radiative flux to the wall for all cases, regardless of the process, occurs in the spectral region above 2000 Å. As was expected, most of the flux below 2000 Å was absorbed. In Fig. 2a, the flux between 800 and 2000 Å is plotted by case. By comparing this with Figs. 1a–1f, it is noted that while this region is dominated by atomic nitrogen lines, not all nitrogen lines occur below 2000 Å. In contrast, Fig. 2b examines the flux above 2000 Å. No region of strong absorption was found for any of the cases in this spectral region.

The influence of differing ionization potential energies was minimal. Examination of Figs. 1a and 1b reveals only a minor decrease in the flux resulting from atomic nitrogen in the I2K2S1 case. In this case, ionization is assumed to take place directly from the ground state. This leads to a less efficient energy transfer between the vibrational-electronic energy mode and the translational-rotational mode. As a result, there is a minor decrease in the vibrational temperature that has been assumed to be equivalent to the electron temperature. Since the electron temperature controls most atomic radiative processes, there is a slight decrease in radiative flux resulting from the assumption that ionization takes place from the ground state.

By contrast, the variation of the kinetic model produced wide differences in the resulting radiative flux profiles. When Figs. 1c and 1d are compared with the baseline case in Fig. 1a, the differences are obvious. The I1K3S1 case experiences a dramatic increase in the radiative flux resulting from atomic nitrogen processes. In addition, the I1K3S1 case is the only

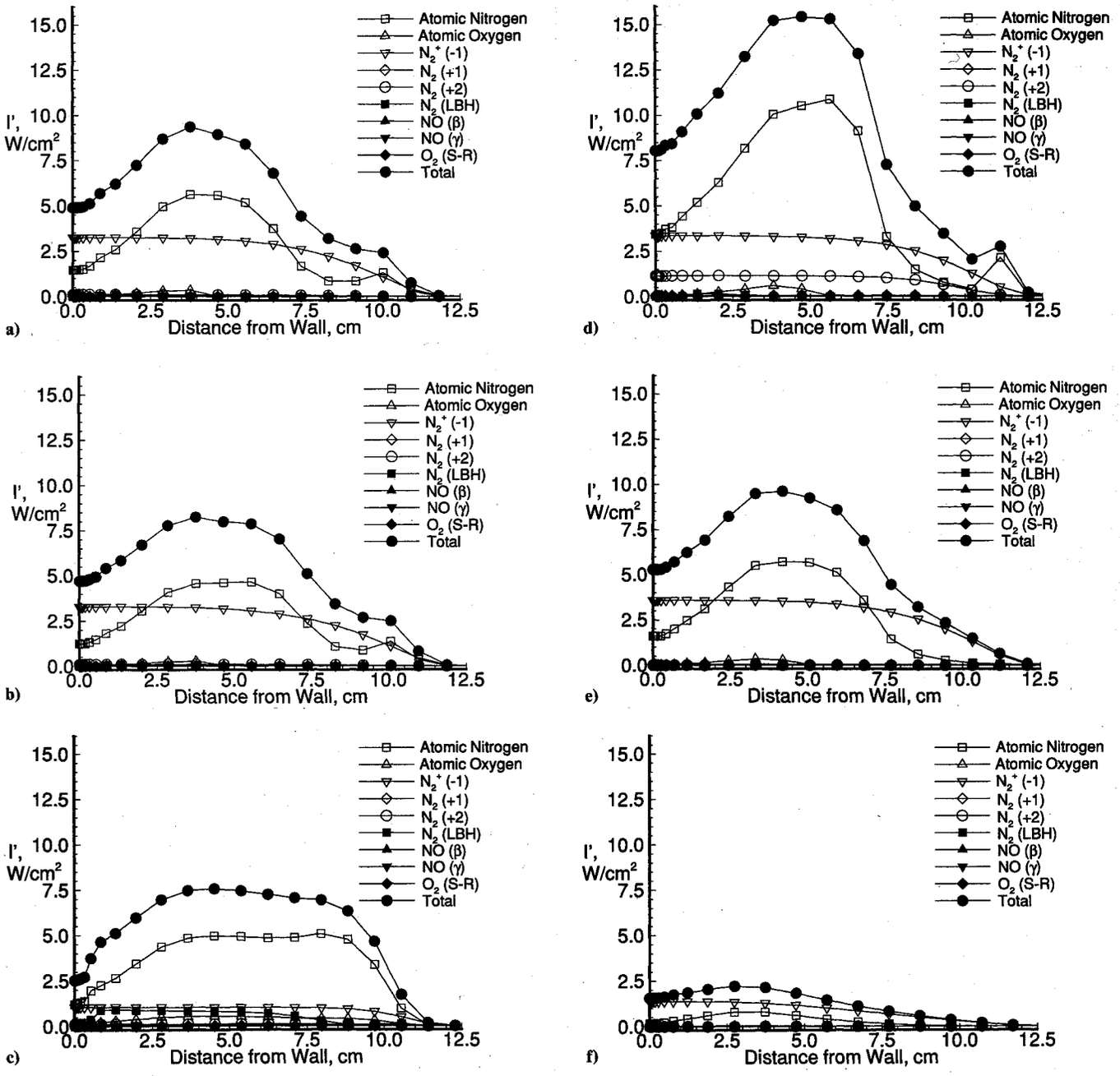

Fig. 1 Kinetic model effect on shock layer radiative flux distributiona at $V_\infty = 9.69$ km/s, $\rho_\infty = 2.48$ kg/m^3: a) baseline (I1K2S1) case, b) I2K2S1 case, c) I1K1S1 case, d) I1K2S1 case, e) I1K2S2 case, and f) I1K2S3 case.

case showing significant radiation in the N_2 second positive band resulting from $C^3\Pi \rightarrow B^3\Pi$ transitions. The variation in atomic radiation is believed to be primarily due to the increase in T_V, Fig. 3b, seen in the I1K3S1 case. Figure 4a examines the atomic nitrogen radiative flux on a case by case basis, while Fig. 4b examines the corresponding atomic nitrogen number densities. There is little variation in number density whereas there are significant differences in the vibrational-electronic temperatures. The flux from the N_2^+ first negative band remains virtually the same between the two cases utilizing Park's chemical rates.

When the I1K1S1 (Kang and Dunn's chemical rates) case is compared with the baseline case, substantial differences are again evident. The flux from N_2^+ is reduced to a contribution to the wall of approximately 1 W/cm^2. In Fig. 5a, where N_2^+ first negative radiation is examined, the Kang and Dunn rates show a dramatically reduced profile relative to the other cases. The reason for this is shown in Fig. 5b. The N_2^+ concentrations are approximately an order of magnitude lower for the Kang and Dunn rates as compared with either set of Park's rates. The atomic nitrogen radiative profile of the I1K1S1 cases differs from the baseline case in that the radiative flux increases much more rapidly and peaks at approximately 10 cm from the wall, maintaining a flat profile throughout the majority of the shock layer.

The variation of the limiting cross section for vibrational excitation σ_V from the baseline curve fit of Park produces few surprises. In Fig. 1e, radiative profiles strongly resemble those of the baseline case with the only exception being the absence of the atomic nitrogen peak in the immediate postshock region as already discussed. Figure 1f indicates that at $\sigma_V = 1 \times 10^{-17}$ little radiation takes place. The N_2^+ first negative again dominates this case, yet total radiative flux is only approximately 1.6 W/cm^2 at the wall. It is interesting that, although this case produces the highest concentrations of N_2^+ of all of the cases studied (Fig. 5b) it has the lowest radiative flux.

Although radiation from N_2^+ is highly dependent on the concentration of N_2^+, radiation in this case is subdued by the low T_V as seen in Fig. 3b.

Also, it is important to examine several interesting features about the state populations of the I1K2S1 baseline case. In Fig. 6a, the state populations for the five N_2 states evaluated by the NEQAIR code are presented for this case. The patterns illustrated are typical of the state populations for O_2, NO, and both atomic nitrogen and oxygen. A Boltzmann distribution assuming that the five states presented are the only states for the N_2 molecule and calculated with the controlling temperature of T_V is presented for comparison. Although this is not accurate, N_2 having far more states, the Boltzmann distribution reflects the same methodology as NEQAIR, which also allocates the total population of N_2 among only the five states presented.

Excited state populations rise rapidly as the T_V begins to peak. After T_V peaks and begins to decline, the increase in flowfield density as the boundary layer is approached begins a second increase in excited state number densities. At approximately 0.5 cm from the wall, the same point where the flowfield became transparent to radiation, excited state populations as calculated by NEQAIR begin to rapidly increase relative to the calculated Boltzmann populations. Again, this pattern was typical for other species with the exception of N_2^+. Note that the state populations calculated by NEQAIR are

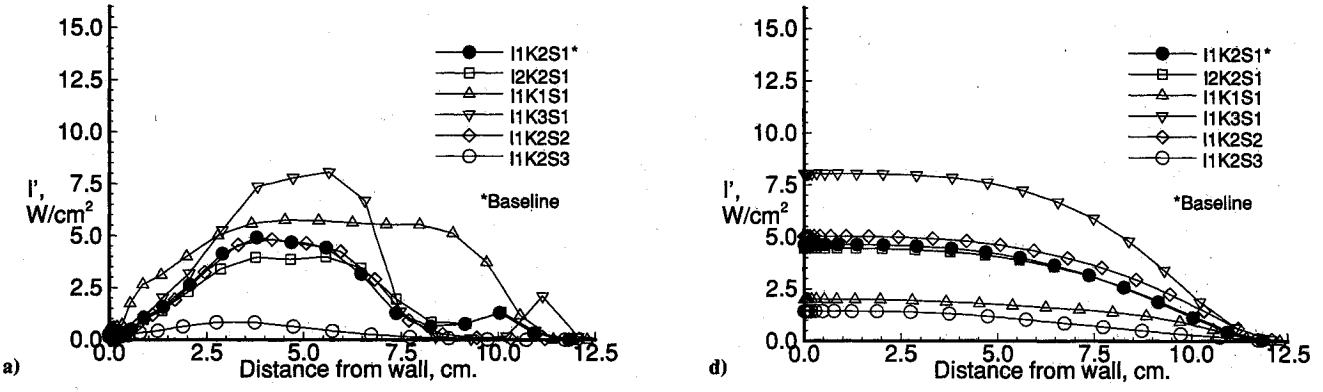

Fig. 2 Shock layer radiative flux distribution over a spectral range at $V_\infty = 9.69$ km/s, $\rho_\infty = 2.48$ kg/m^3: a) wavelengths below 2000 Å and b) wavelengths below 2000 Å.

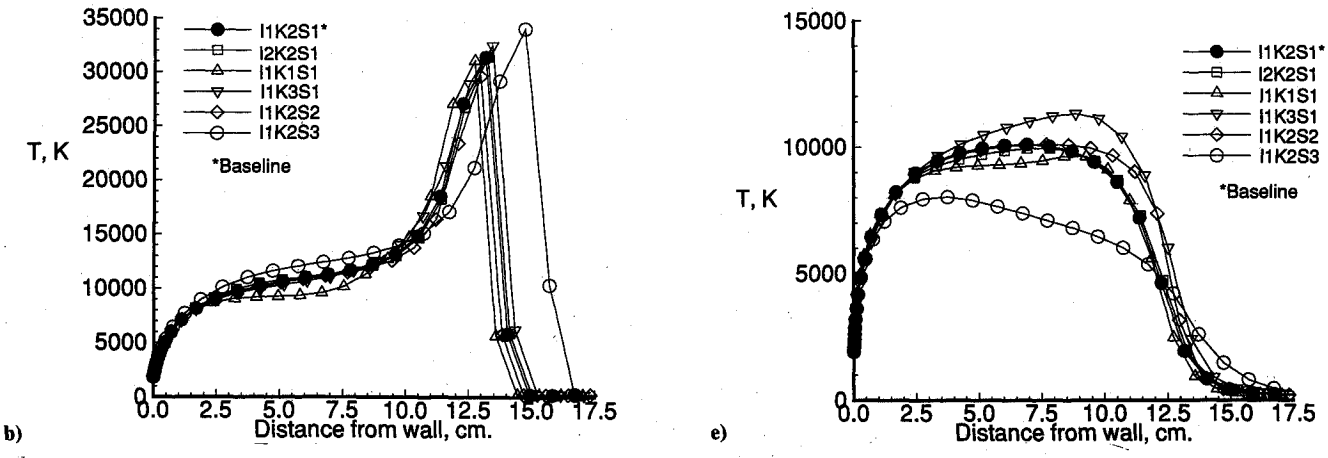

Fig. 3 Kinetic model effect on shock layer temperature distribution at $V_\infty = 9.69$ km/s, $\rho_\infty = 2.48$ kg/m^3: a) translational temperature and b) vibrational temperature.

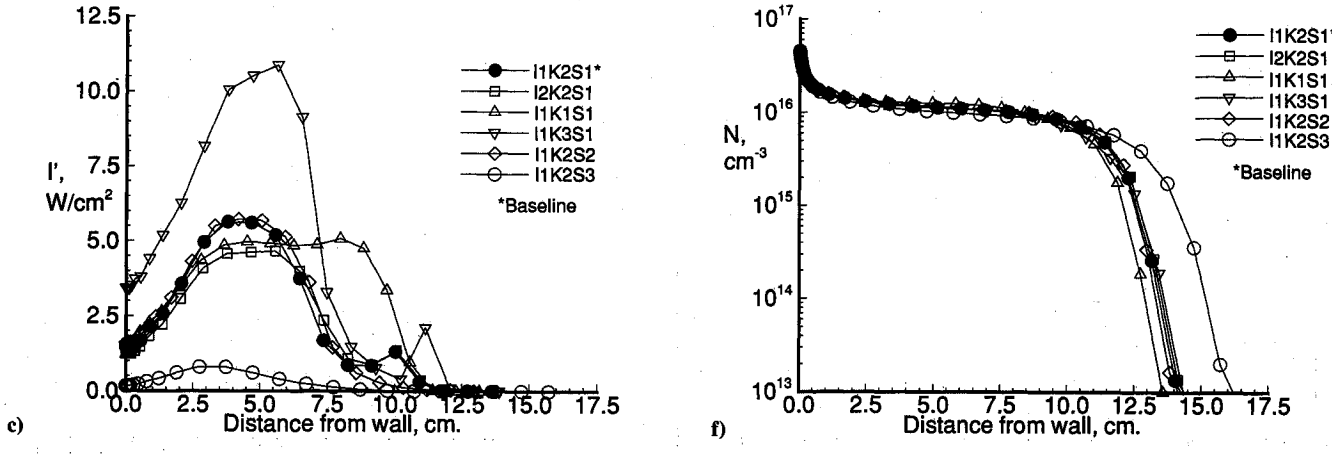

Fig. 4 Kinetic model effect on atomic nitrogen at $V_\infty = 9.69$ km/s, $\rho_\infty = 2.48$ kg/m^3: a) radiative flux and b) number densities.

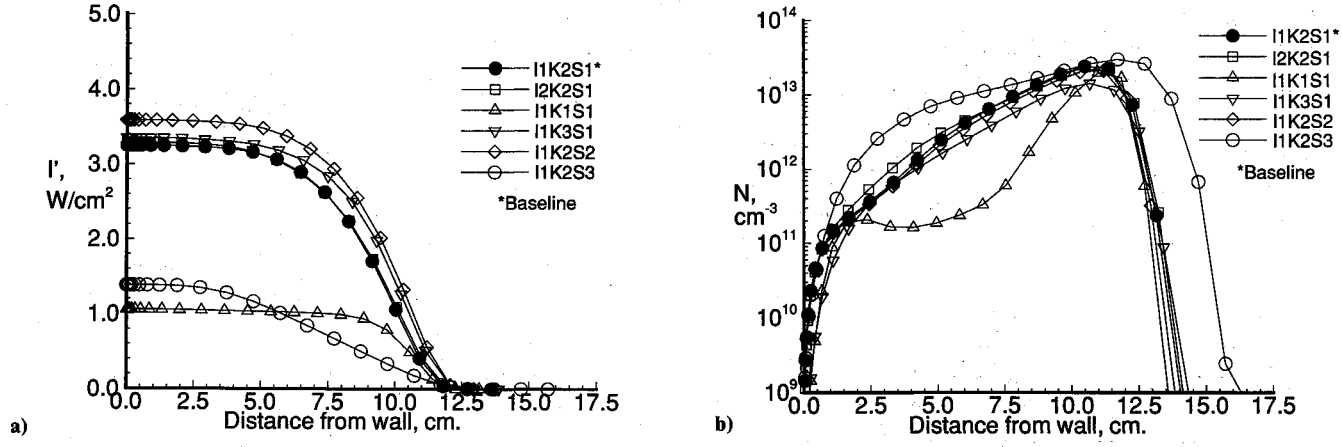

Fig. 5 Kinetic model effect on molecular nitrogen at $V_\infty = 9.69$ km/s, $\rho_\infty = 2.48$ kg/m^3: a) radiative flux and b) number densities.

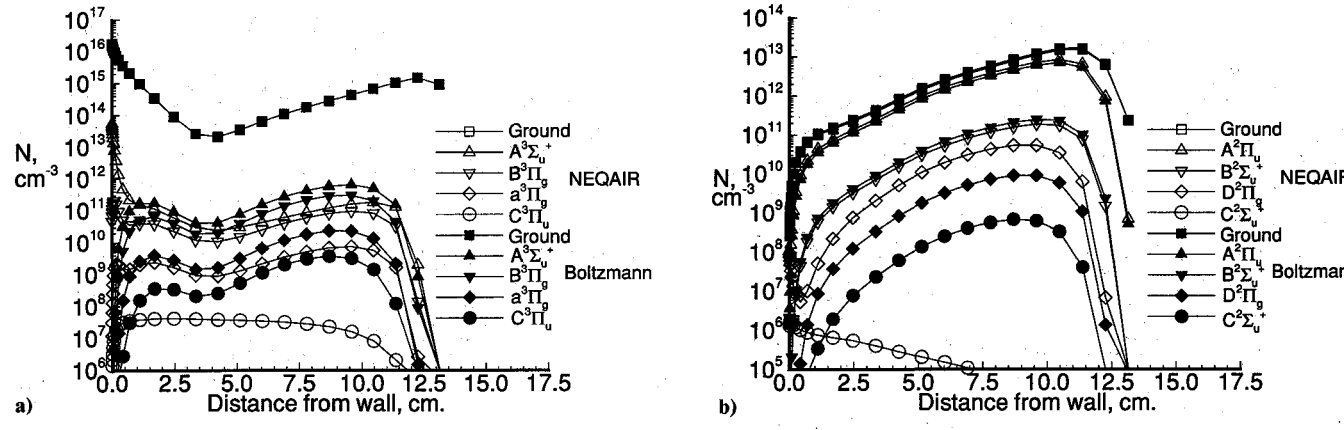

Fig. 6 State population distributions at $V_\infty = 9.69$ km/s, $\rho_\infty = 2.48$ kg/m^3: a) N_2 state population distribution b) N_2^+ state population distribution.

also lower than the same state's population calculated by a Boltzmann distribution. However, when the state populations of N_2^+ are examined in Fig. 6b, the excited state populations for the four lowest states are approximately at or, for some states, above their Boltzmann distribution values. It should be noted that, due to the similarity in magnitude between the excited state populations and the Boltzmann values, it is very difficult to separate the lines in this figure. Since this pattern was found for all of the case's N_2^+ populations and is in direct conflict with the pattern displayed by the other species, it is reasonable to conclude that the high excited state populations of this molecule relative to the other radiating species state populations are responsible for the fact that radiation from N_2^+ constitutes, on the average, 50% of the total radiative flux to the wall.

Trajectory Variations

From Table 1, the aeroassist vehicle is at the closest point to entry into the continuum flow regime in this study at an altitude of 82.96 km. The radiative flux at this point is close to its peak value for this trajectory. Total radiative flux to the wall is 5.97 W/cm^2, and the flux to the wall is roughly divided in half for atomic nitrogen processes and for N_2^+ first negative radiation. As in the preceding section, radiative flux becomes transparent in the interior boundary layer. The location of peak incident radiation corresponds to the location of peak flux for atomic nitrogen at 7.5 cm from the wall. The peak atomic nitrogen radiative flux lags the peak value of T_V by almost 2.5 cm as was also seen in Figs. 3b and 4a.

The peak convective heating point was reached at $t = 110$ s. The radiative flux was again divided roughly in half between atomic nitrogen processes and the N_2^+ first negative band radiation for a total flux to the wall of 6.12 W/cm^2. Although the actual peak radiative flux for all of the cases studied occurred at $t = 90$ s, this case was not presented in this paper due to its radiative similarity to the $t = 70$ s point and the fact that total radiative flux to the wall was only 0.2 W/cm^2 greater. The higher density at $t = 110$ s leads to more efficient equilibration in the shock layer. Peak radiative flux becomes more defined and moves to 9.5 cm from the wall, lagging the peak vibrational temperature by only 1 cm.

In Fig. 7c the lowest altitude case for this study is presented. At $t = 150$ s, the altitude is 75.03 km and velocity has slowed to 8.744 km/s. Total radiative flux to the wall is 3.03 W/cm^2, with atomic nitrogen contributing 1.14 W/cm^2 and N_2^+ first negative providing 1.89 W/cm^2 of the total flux.

Similarly, as the vehicle begins to exit the atmosphere at $t = 190$ s, the radiative flux (Fig. 7d) to the wall has decreased to a total flux of 1.06 W/cm^2. The atomic nitrogen contributes 0.27 W/cm^2 and N_2^+ first negative contributes 0.71 W/cm^2 to the total. The altitude at this point is 76.15 km with a velocity of 8.145 km/s.

Throughout the examination of trajectory point variations there were few surprises. Atomic nitrogen and N_2^+ first negative radiative processes dominated the radiative structure with peak total radiative heating occurring before the peak convective heating point at $t = 110$ s. The variation of velocity and altitude within the scope of this study yielded no increases in

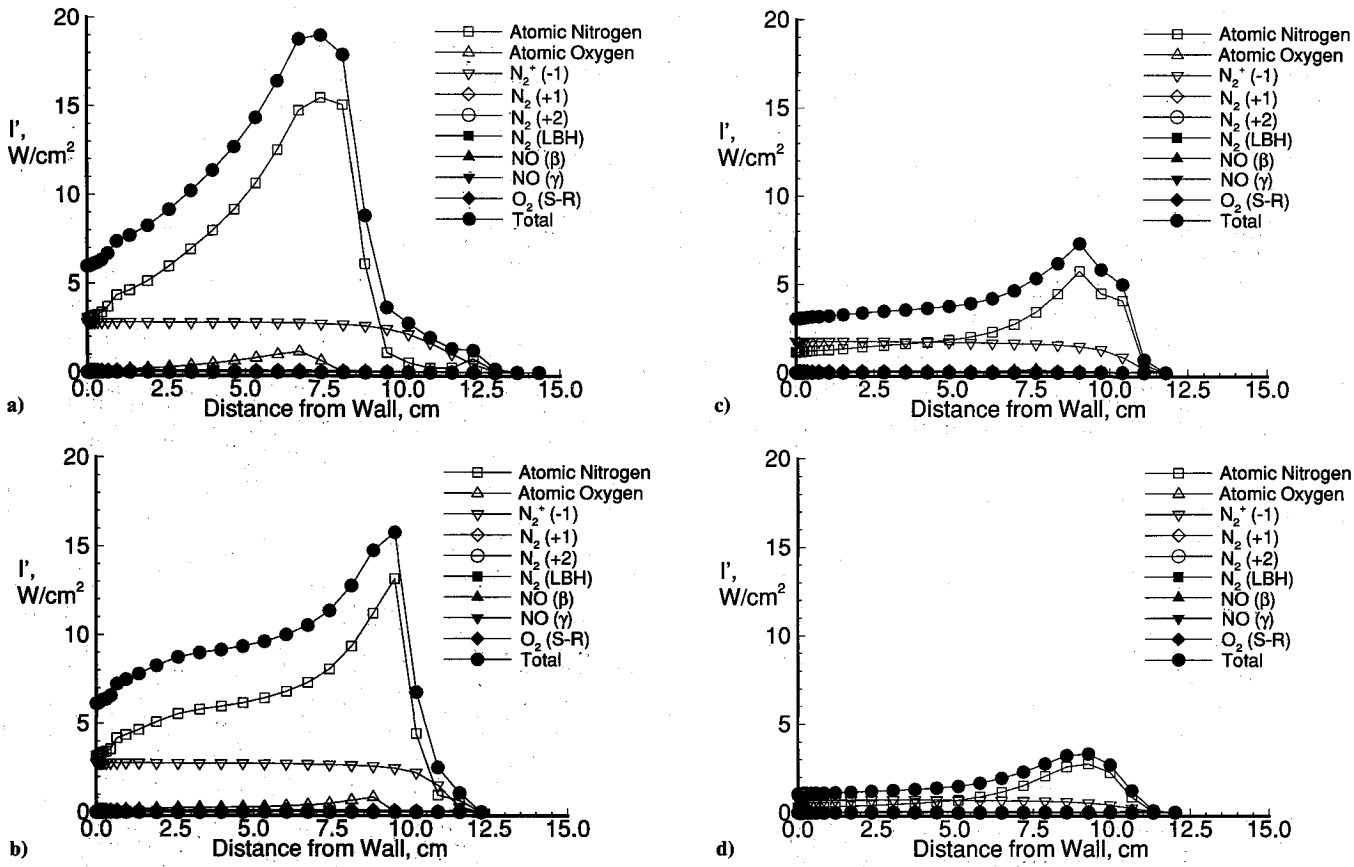

Fig. 7 Radiative flux by altitude variation: a) t = 70 s, altitude = 8.96 km, b) t = 110 s, altitude = 76.47 km, c) t = 150 s, altitude = 75.03 km, and d) t = 190 s, altitude = 76.15 km.

the other radiative processes calculated by the NEQAIR code. However, this result should not be generalized to other vehicles or trajectories.

Concluding Remarks

Variation of the kinetic model parameters for a flowfield calculation produced several interesting results. Changing the ionization potential energy to include ionization from the ground state as opposed to occurring from an already excited state resulted in a minor reduction on the radiative flux resulting from atomic nitrogen without any effect on other radiative processes. By contrast, changing the chemical rate model had a substantial influence not only on the magnitude but also on the structure of the radiative processes. Variation of the limiting vibrational excitation cross section yielded significant variations in the observed radiative fluxes only in their magnitude; no substantial changes were found in the overall structure and composition of the radiative fluxes. For a variation in freestream conditions and with the chemical rates fixed at Park's (1987) rates, radiative composition did not change substantially. Only the magnitude of the radiative flux varied. It is reasonable to assume that other chemical rate models would also retain their unique radiative structures throughout a similar trajectory. These results would imply that spectral flight data might help determine the appropriateness of the chemical rate models used in the solution of such flowfields. It is not felt that flight data would be of use in determining which ionization or σ_V model would be best for a flowfield solution method due to the minor differences, other than magnitude, observed in this study. Although variations in radiative magnitude could be caused by a variety of influencing factors, in this study it appears that changes in radiative structure and composition between flight and calculated data would only be caused by variations between actual shock layer chemistry and calculated chemistry.

The fact that the interior boundary layer of all of the flows became transparent to radiative flux is not necessarily intuitive. One would expect that this region of the flow with higher densities and lower temperatures would account for the majority of the absorption taking place. In addition, most of the species studied in this region experienced an overpopulation relative to their corresponding Boltzmann distributions. It is certainly possible that this is purely a computational problem resulting from the lack of sufficiently appropriate excitation rates at low temperatures. Another explanation could result from the wall boundary condition. The requirement that all temperatures be equal at the wall at a user-defined value may be adequate from a macroscopic perspective yet incorrect on a microscopic basis. There is, of course, the possibility that the effect is real and results from particles recombining into excited states that do not make a transition down to their respective ground states. This would lead to highly populated excited states that are not in a position to absorb incoming photons. A related observation was the high population of the excited states of N_2^+. Again, this may be due to inappropriate excitation rates. The problem is more significant here given the predominance of the N_2^+ first negative band in the radiative structure and the fact that this occurs throughout the shock layer, not just in the interior boundary layer.

Finally, due to the computational complexity of the NEQAIR code and the computational time required in obtaining solutions similar to those used in this study, it is recommended that the number of radiative processes included in the NEQAIR code be reduced. For similar flowfields, the only radiative processes that need to be included in the solution routine are N_2^+ first negative, N_2 second positive, and atomic nitrogen and oxygen processes.

Acknowledgments

This work was sponsored by NASA under Contract NAS1-19237. The author wishes to thank the technical monitor, David Throckmorton, for his support. In addition, the author would like to thank Chul Park for providing the latest version of the NEQAIR code and Peter Gnoffo for providing some of the flowfields used in this study.

References

[1]Park, C., "Nonequilibrium Air Radiation (NEQAIR) Program: User's Manual," NASA TM 86707, July 1985.

[2]Greendyke, R.B., and Hartung, L.C., "An Approximate Method for the Calculation of Nonequilibrium Radiative Heat Transfer," *Journal of Spacecraft and Rockets,* Vol. 28, No. 2, 1991, pp. 165-171.

[3]Hartung, L. C., "Nonequilibrium Radiative Heating Prediction Method for Aeroassist Flowfields with Coupling to Flowfield Solvers," Ph.D. Thesis, Dept. of Mechanical and Aerospace Engineering, North Carolina State Univ., Raleigh, NC, 1991.

[4]Jones, J. J., "The Rationale for an Aeroassist Flight Experiment," AIAA Paper 87-1508, June 1987.

[5]Gnoffo, P. A., Gupta, R. N., and Shinn, J., "Conservation Equations and Physical Models for Hypersonic Air Flows in Thermal and Chemical Nonequilibrium," NASA TP 2867, Feb. 1989.

[6]Gnoffo, P. A., "Upwind-Biased, Point-Implicit Relaxation Strategies for Viscous, Hypersonic Flows," AIAA Paper 89-1972, June 1989.

[7]Greendyke, R. B., Gnoffo, P. A., and Lawrence, R. W., " Electron Number Density Profiles for the Aeroassist Flight Experiment," AIAA Paper 92-0804, Jan. 1992.

[8]Roe, P. L., "Approximate Riemann Solvers, Parameter Vectors, and Difference Schemes," *Journal of Computational Physics,* Vol. 43, No. 2, 1981, pp. 357-372.

[9]Harten, A., "High Resolution Schemes for Hyperbolic Conservation Laws," *Journal of Computational Physics,* Vol. 49, No. 3, 1983, pp. 357-393.

[10]Yee, H. C., "On Symmetric and Upwind TVD Schemes," NASA TM 86842, Sept. 1985.

[11]Yee, H. C., "Numerical Experiments with a Symmetric High-Resolution Shock-Capturing Scheme," NASA TM 88325, June 1986.

[12]Kolodziej, P., and Stewart, D. A., "Nitrogen Recombination on High-Temperature Reusable Surface Insulation and the Analysis of its Effect on Surface Catalysis," AIAA Paper 87-1637, June 1987.

[13]Kang, S. W., and Dunn, M. G., "Theoretical and Measured Electron Density Distributions for the RAM Vehicle at High Altitudes," AIAA Paper 72-689, June 1972.

[14]Park, C., "Assessment of Two-Temperature Kinetic Model for Ionizing Air,"AIAA Paper 87-1574, June 1987.

[15]Park, C., *Nonequilibrium Hypersonic Aerothermodynamics,* Wiley, New York, 1990.

[16]Hansen, C. F., "Collision-Induced Gas Phase Dissociation Rates," Final Rept. NASA Grant NAG1-1046, Aug. 1990.

[17]Arnold, J. O., Whiting, E. E., and Lyle, G. C., "Line By Line Calculation of Spectra from Diatomic Molecules and Atoms Assuming a Voight Line Profile," *Journal of Quantitative Spectroscopy and Radiative Transfer,* Vol. 9, No. 6, 1969, pp. 775-798.

Ernest V. Zoby
Associate Editor